Retrofugal Electron Flux from Massive Targets Irradiated with a Monoenergetic Primary Beam*

RALPH W. DRESSEL
Department of Physics, New Mexico State University, University Park, New Mexico
and
Nuclear Effects Laboratory, White Sands Missile Range, New Mexico
(Received 21 June 1965; revised manuscript received 20 October 1965)

Nearly monoenergetic electrons in a collimated beam have been directed at normal incidence onto a variety of thick targets ranging in atomic number from Be to U. The ratio $r(\theta,E_0,Z)$ of the number of retrofugal (i.e., energetic secondary plus backscattered primary) electrons per steradian to the number of incident primaries has been measured for a total of 11 targets. The mean energy E_0 of the incident electrons was varied from 0.5 to 10 MeV and the dependence of r upon θ explored for angles between 90° and 180° with respect to the forward beam axis. For targets having $Z\geq 29$ the angular distributions are independent of E_0 and are described by $\cos^{1.35}\theta$; but for targets with $Z\leq 13$, $r(\theta,E_0,Z)$ depends upon all three parameters. Typical values obtained for the retrofugal flux coefficient range from $r(180°, 10\text{ MeV}, 4)=1.2$ milliunits/steradian for Be to $r(180°, 0.5\text{ MeV}, 92)=274$ for U. These generally are higher than those reported previously.

INTRODUCTION

THE interaction of energetic electrons with other elemental systems is moderately well understood and, except for fine details, many features of the transport of electrons in bulk matter can be calculated from known cross sections. Much work already has been done in this regard and a number of comprehensive review articles dealing with the passage of electrons through matter have appeared in the literature.[1–7] These indicate that, in general, there is good agreement between theoretical models and measurements concerning both energy loss and the associated distribution of ionization in homogeneous absorbers. Also, multiple and plural scattering in absorbing layers much thinner than the electron range has acquired a satisfactory theoretical treatment.[8] But no comparable coverage of the scattering of electrons incident upon a plane interface between dissimilar extended media has been developed. An attempt to calculate the return electron flux directly from the successive discrete interactions quickly becomes suffocated in the enormous number and variety of stochastic encounters experienced by any given electron. To render such calculations tractable, alternative approaches have been used which simulate the detailed process by considering it as a diffusion phenomenon,[9–14] by introducing simplifying approximations to the physical problem,[15] by application of a principle known as *invariant imbedding*,[16] or by Monte Carlo methods in which the detailed history of an electron in its progress through a medium is replaced by a relatively small number of steps, each of which represents the cumulative effect of many encounters.[17–21]

The early experimental investigations of electron back-scattering from thick targets have been summarized in review articles by Lenard and Becker,[1] Bothe,[2] and Birkhoff.[5] More recent work by numerous experimenters has extended the data for a large variety of target materials over an energy range from 200 eV to 22 MeV.[22–33] However, only Kulenkampff,[22,23] Kanter,[24] and Frank[28] have reported information about the angular distribution of backscattered electrons. Measurements presented here provide additional data on

* This work was supported in part by a grant from the U. S. Army Research Office, Durham and, in part, by a grant from the National Aeronautics and Space Administration.

[1] P. Lenard and A. Becker, *Handbuch der Experimental Physik* (Wien und Harms, Leipzig, 1927), Bd. 14, S. 337.
[2] W. Bothe, *Handbuch der Physik* (Springer-Verlag, Berlin, 1933), Bd. 24, Teil. 2, S. 1.
[3] H. Bethe and J. Ashkin, *Experimental Nuclear Physics* (John Wiley & Sons, Inc., New York, 1953), Vol. I.
[4] W. Paul and H. Steinwedel, *Beta- and Gamma-Ray Spectroscopy* (Interscience Publishers, Inc., New York, 1955).
[5] R. D. Birkhoff, *Handbuch der Physik—Encyclopedia of Physics* (Springer-Verlag, Berlin, 1958), Vol. 34, p. 53.
[6] R. M. Sternheimer, *Methods of Experimental Physics* (Academic Press Inc., New York, 1961), Vol. 5A, p. 1.
[7] U. Fano, Natl. Acad. Sci.—Natl. Res. Council, Publ. No. 1133.
[8] W. T. Scott, Rev. Mod. Phys. **35**, 231 (1963).
[9] W. Bothe, Ann. Physik **6**, 44 (1949).
[10] G. D. Archard, J. Appl. Phys. **32**, 1505 (1961).
[11] R. Englemann, Nukleonik **3**, 147 (1961).
[12] Z. T. Bödy, Brit. J. Appl. Phys. **13**, 483 (1962).
[13] S. G. Tomlin, Proc. Phys. Soc. (London) **82**, 465 (1963).
[14] H. W. Thümmel, Z. Physik **179**, 117 (1964).
[15] T. E. Everhart, J. Appl. Phys. **31**, 1483 (1960).
[16] R. F. Dashen, Phys. Rev. **134**, A1025 (1965).
[17] T. Sidei, T. Higasimura, and K. Kinosita, Mem. Fac. Eng. Kyoto Univ. **19**, 220 (1957).
[18] C. MacCallum, Bull. Am. Phys. Soc. **5**, 379 (1960).
[19] M. Green, Proc. Roy. Soc. (London) **82**, 204 (1963).
[20] J. F. Perkins, Phys. Rev. **126**, 1781 (1962).
[21] M. J. Berger, *Methods in Computational Physics* (Academic Press Inc., New York, 1963), Vol. I.
[22] H. Kulenkampff and W. Spyra, Z. Physik **137**, 416 (1954).
[23] H. Kulenkampff and K. Rüttinger, Z. Physik **137**, 426 (1954).
[24] H. Kanter, Ann. Physik **20**, 144 (1957).
[25] J. Holliday and E. Sternglass, J. Appl. Phys. **28**, 1189 (1957).
[26] B. Agu, T. Burkett, and Matsukawa, Proc. Phys. Soc. (London) **71**, 201 (1958); **72**, 727 (1958).
[27] Yu. A. Simchenko, Radiotekhn. i Elecktron. **4**, 1381 (1959).
[28] H. Frank, Z. Naturforsch. **12a**, 780 (1957); **14a**, 247 (1959).
[29] K. Wright and J. Trump, J. Appl. Phys. **33**, 687 (1962).
[30] J. Bienlein and G. Schlosser, Z. Physik **174**, 91 (1963).
[31] E. Weinryb and J. Philibert, Compt. Rend. **258**, 4535 (1964).
[32] D. Harder and H. Ferbert, Phys. Letters **9**, 233 (1964).
[33] K. Koral and A. Cohen, NASA Tech. Note TN D-2782 (1965); TN D-2909 (1965).

the angular distribution of these return electrons for a greater number of targets and for a larger range of energies than have been previously reported. They also indicate significantly higher values for the relative number of electrons returning from an irradiated target face. Possible reasons for this discrepancy will be examined in detail.

A collimated beam of monoenergetic electrons directed at a thick target will sustain a variety of interactions with the constituent atomic nuclei and their associated atomic electrons to produce a large dispersal of the original beam. Part of this dispersal comes from single Coulomb scattering; however, most of it results from multiple inelastic scattering which produces a broad diffusion of the electrons. In addition, energy and momentum are transmitted to resident electrons in the target medium by direct electron-electron encounters and through secondary processes such as Compton collisions with bremsstrahlung previously generated within the target by the primary beam. Photoelectrons and positron-electron pairs may appear as well. Thus, the total number of energetic electrons in the system may exceed the number introduced by the incident beam. The relative contributions from these numerous components depend strongly upon the primary electron energy and also upon the atomic number of the target material. As part of the total transport within the medium, some electrons will migrate close enough to the target surface to escape. These constitute an electron flux directed backward with respect to the incident beam and commonly have been called *backscattered* electrons. However, from the previous discussion it is evident that scattering contributes only part of the return electron flux. A smaller but apparently significant portion is furnished by the secondary processes. For this reason, it seems appropriate to introduce *retrofugal flux* as a new term that includes within its denotation the energetic secondary electrons as well as the scattered primaries returning from a target. By universal convention, the very low-energy component identified as secondary-emission electrons is excluded. These are emitted from the target surface with energies less than 50 eV.[33,34] While such secondary-emission electrons can be discriminated experimentally on the basis of energy, the scattered primary and energetic secondary electrons are indistinguishable. Accordingly, all electrons leaving the target surface with energies greater than the cutoff energy are experimentally equivalent. These constitute the retrofugal flux.

EXPERIMENTAL SYSTEM

The system employed for measuring the retrofugal electron flux is illustrated in Fig. 1. A large cylindrical scattering chamber approximately 30 cm in diameter and 30 cm high was constructed of aluminum to reduce the background effects due to electrons scattered around its interior. Targets were fabricated as solid right-circular cylinders approximately 5 cm in diameter and 5 cm long. They were supported in an aluminum holder and mounted so that the center of the plane-end face lay precisely at the center of the scattering chamber. The holder permitted target rotation about a vertical axis so that it could be positioned at any angle with respect to the incident beam. The target surface exposed to the beam was machined plane within $\pm 25\ \mu$. Ten measurement ports were spaced around the scattering chamber periphery. By rotating the chamber it

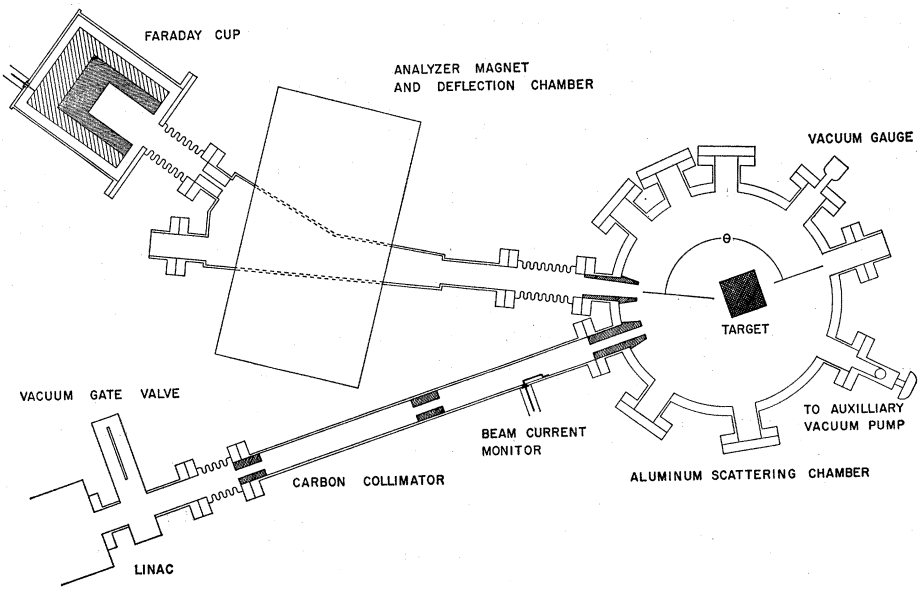

FIG. 1. Arrangement of apparatus for measuring the retrofugal flux of electrons from massive targets.

[34] A. Schultz and M. Pomerantz, Phys. Rev. **130**, 2135 (1963).

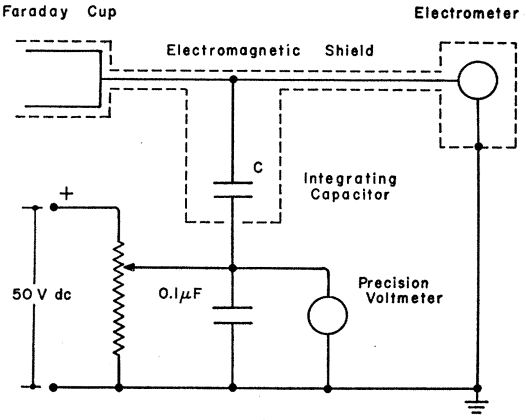

FIG. 2. Schematic diagram of the electrical circuit for measuring accumulated charge on the Faraday cup.

was possible to select appropriate pairs of ports to obtain regularly increasing deflection angles from 0° to 155° at 5° intervals. Thus, 32 angular intervals were available with only 10 ports. Target materials have been chosen to span the scale of atomic numbers at reasonably uniform intervals from the low end at $Z=4$ for beryllium to the high end at $Z=92$ for uranium. Only good metallic conductors have been selected for targets to avoid accumulation of electric charge and to conduct away heat generated by the incident beam.

Electrons leaving the S-band Linac passed through a system of aligned collimating apertures in a drift tube. This same drift tube contained a beam-current monitor[35] which was calibrated, with the target removed, against a Faraday cup mounted at the straight-through port. Although the Linac current was reasonably steady so that measurements of relative currents were feasible, greater precision was obtained by comparing the integrated monitor current against the total charge collected by the Faraday cup.

The output of the Faraday cup was carried through a coaxial cable to an integrating capacitor at the input of a sensitive electrometer located outside the irradiation room. A schematic diagram of the electrical system employed is shown in Fig. 2. During an exposure, the sliding bias on the integrating capacitor was manually adjusted to keep the electrometer always at null. Then, after a predetermined number of pulses, the bias voltage required for the electrometer null indication was read from a calibrated $\frac{1}{4}\%$ precision voltmeter. In tracking the null, the electrometer was kept within ± 0.2 V from zero. Such tight control was not necessary since the shunt resistance to ground was greater than 10^{11} Ω, but it was easy to achieve and it ensured that the errors caused by leakage and ionization currents at the Faraday cup were less than an equivalent of 0.003 milliunit/sr. The integrating capacitor together with the capacitance of the Faraday cup, its cable, and the electrometer input were measured in place with an impedance bridge having an accuracy of $\pm 0.1\%$. Zero drift of the electrometer was negligible. Since the incident-beam monitor was calibrated with this same system and since the final results are expressed as a ratio, the instrument calibrations all cancel. Thus, not the instrument characteristics but only the geometrical configuration influenced the final determination of the relative electron flux. Basically, the values of two readings on the same voltmeter for equal numbers of pulses were compared and this ratio was divided by the solid angle subtended at the target by the detector to determine the retrofugal-flux coefficients. Effectively, electrons were counted by means of the charge collected by the Faraday cup and the final result expressed the electron-flux ratio directly as long as the system characteristics remained stable. This critical detail was checked periodically during the course of the measurements and at no time did any of the calibrations shift outside the limits of precision quoted. An evaluation of the errors and charge losses expected from secondary radiation and scattering from the Faraday cup indicates that they are less than 0.2%.[36] Immediate repetition of monitor calibration readings gave results consistent within 0.5%. Unfortunately, due to random fluctuations in the many parameters that determine the Linac operating condition this high precision could not be held over a period longer than a few minutes. However, these fluctuations had a standard deviation of about 5% so that averages over several replications yielded results reliable within 2 or 3%.

Although the primary beam formed by the Linac had a cross section not greater than 2 mm in diameter, the beam itself migrated during the irradiation period and executed an excursion over a region about 5 mm in diameter. The carbon collimators were designed with apertures 1 cm in diameter so that, when properly aligned, the electron beam always remained within these apertures. The solid angle through which the retrofugal electron flux was sampled was defined by another carbon cylindrical collimator having a conical taper matching the solid-angle cone subtended at the target. This collimator viewed the entire region on the target face from which retrofugal electrons were emitted. When measurements of the energy spectra were desired the analyzer magnet and deflection chamber were installed as shown. Alternatively, when only the electron flux per unit solid angle without energy analysis was desired, the Faraday cup was coupled directly to the appropriate measurement port. The entire assembly, including the scattering chamber and Faraday cup, was evacuated and connected directly to the Linac system which operated at a pressure of about 10^{-7} Torr.

Test measurements have been performed to check out the system for background signals, leakage currents, and other spurious effects. The scattering chamber itself

[35] R. Dressel, Nucl. Instr. Methods 24, 61 (1963).

[36] R. Dressel, Nuclear Effects Laboratory Report, 1961 (unpublished).

was tested by placing a uranium target in the beam but at the extreme end where electrons issuing from it could not reach the Faraday cup directly. However, the scattered electrons then flooded the chamber interior and presumably some of these could enter the detector. The signal generated by this source, when reduced to terms useful for evaluation, was less than 0.05 milliunit/sr. Since for uranium the return electron flux is about 100 milliunit/sr, this much relative background due to scattering was negligible. With the target in its normal position, electrons scattered from the chamber walls may fall again on the target face, effectively augmenting the incident beam. An estimate of the upper limit for the error associated with this effect is 0.3% with a uranium target. All other targets contribute a smaller error. Such scattering within the chamber normally would cause the experimental results to be high, but by direct empirical evaluation and by calculation this error proves to be negligible.

The Faraday cup itself was expected to be quite insensitive to any radiation except those electrons entering through its aperture. But, interestingly, with the target absent, a positive signal was observed at the Faraday-cup terminals. This accumulated positive charge was found to be the result of secondary emission from the exterior surface of the lead cup caused by broadside irradiation with stray bremsstrahlung from the Linac. The effect was small and was further reduced by appropriate shielding of the system so that even with the target in place the final equivalent magnitude was less than 0.2 milliunits/sr. Another effect, approximately equal in magnitude, was caused by polarization of the dielectric in the coaxial cables subjected to the radiation field. This gave a negative signal which tended to compensate the small positive error from the cup. Careful determination of these background signals, including charge loss due to leakage currents, showed they were negligible for measurements on targets having atomic numbers greater than 13. For targets of Al, C, and Be, however, positive background-signal corrections of 3, 9, and 21%, respectively, were applied in reducing the data. A Faraday cup was chosen for the detector in this measurement, partly because of its relative insensitivity to spurious background radiations which are inherently high in the presence of the target bremsstrahlung, and partly because it is an absolute instrument. Thus, many problems have been avoided, such as calibration, or dead time and coincidence losses commonly associated with other detectors.

MEASUREMENT CONDITIONS

The spatial distribution of electrons within a medium irradiated with a collimated beam can be made visible by exposing a block of Plexiglas or Lucite to the beam as a target.[37] After sufficient exposure, a green-orange color is registered in the block thereby recording the

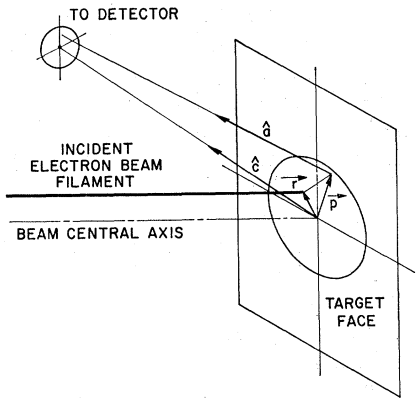

FIG. 3. Diagram defining geometrical parameters at the target.

electron-flux density. From the distribution so indicated it is evident that the lateral spread of the electrons does not extend significantly beyond a circle whose diameter equals the electron range in the material. Therefore, the retrofugal electrons must issue from a similarly limited region on the target centered about the point of entry for the incident beam. As a matter of interest, photographs of the spatial distribution of the retrofugal electrons from targets bombarded with a 45-keV electron beam have been obtained by Schumacher[38] who used the fluorescence induced by the retrofugal electrons in a gas above the target as an indicator.

In the present measurements, the incident-electron beam is distributed over a finite cross-sectional area and has a finite energy spread. Because of this, it is important to define precisely the quantities being measured so that estimates can be made of the systematic errors encountered. Suppose, therefore, as in Fig. 3, that a collimated electron beam is directed normally against a semi-infinite plane target. The incident electron flux density at each position $\mathbf{r}$ on the target face may be expressed as the product of $q(\mathbf{r})$ and N_0, the normalized distribution function and the total number of electrons incident per unit time, respectively. A typical energy spectrum for the incident electrons is shown in Fig. 4. Only small changes in the spectrum

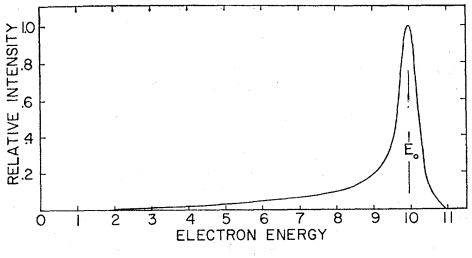

FIG. 4. Energy spectrum of incident electrons. This spectrum profile is typical of the Linac output at the higher energies but as the energy E_0 is decreased the low-energy tail tends to disappear and vanishes completely below 3 MeV.

[37] R. Dressel, Nucl. Instr. Methods 28, 261 (1964).

[38] B. W. Schumacher, Can. J. Phys. 40, 376 (1962).

profile occurred as the energy peak E_0 was changed from 0.5 to 10 MeV but the full width at half-maximum varied slowly from 0.3 MeV at the lower end to 0.6 MeV at the higher end of the energy range. Let ϵ denote the incident electron energy, and let the spectrum of incident energies be represented by $\phi(\epsilon,E_0)$. At these high energies, coherent electron wave interference effects are not significant and only random atomic and nuclear interactions contribute to the beam dispersal.[24] Accordingly, the retrofugal electrons escaping from the target have a broad distribution both in space and in energy which depends upon the site location $\mathbf{p}$ from which they leave and the direction as indicated by the unit vector $\hat{a}$. Let this distribution be described by the function $k[(\mathbf{p}-\mathbf{r}), \hat{a}, E, \epsilon, Z]$ which expresses the relative number of electrons per unit area per steradian per unit energy interval leaving the target with energy E from a position $\mathbf{p}$ and in the direction $\hat{a}$ due to electrons incident at $\mathbf{r}$ with energy ϵ on a target whose atomic number is Z. With these distribution functions it is possible to identify the measured quantities unambiguously. If an aperture is placed at a position $\hat{c}$ with respect to the target as in Fig. 3, then the number of electrons that will pass through it per unit time will be given by the multiple integral

$$N(\hat{c},E_0,Z) = N_0\int_0^\infty\int_0^\infty\int_{\Delta\Omega}\oint\oint q(\mathbf{r})\phi(\epsilon,E_0)k[(\mathbf{p}-\mathbf{r}),\hat{a},E,\epsilon,Z] \times d^2r d^2p d\Omega d\epsilon dE \quad (1)$$

which is carried over the entire target surface and over the solid angle $\Delta\Omega$ subtended at the target by the detector aperture. For an incident beam directed normally against a homogeneous isotropic target, the retrofugal electron flux is symmetrically distributed about the central axis. Under these conditions $N(\hat{c},E_0,Z)$ will depend only upon the angle θ between $\hat{c}$ and the beam central axis. This angle is always greater than 90° for the retrofugal flux. The distribution functions appearing in the integrand are all limited in range; $q(\mathbf{r})$ is confined by the collimators to a circle whose diameter is 1 cm. Moreover, it is expected that $k[(\mathbf{p}-\mathbf{r}), \hat{a}, E,\epsilon, Z]$ will be approximately a Gaussian function of $|(\mathbf{p}-\mathbf{r})|$ having a full width at half-maximum less than the electron range in the target medium. Although the energy spectrum of k is broad, it falls to zero for $E>\epsilon$. Also, by design, the solid-angle interval $\Delta\Omega$ is small. Therefore, the conditions of measurement can be reasonably well established in terms of mean values over the finite extent of the interval ranges.

There are three important coefficients that are particularly useful in describing the retrofugal flux. A differential retrofugal-flux coefficient may be defined in terms of measured quantities by

$$G(\theta,E,E_0,Z)=\frac{N(\theta,E,E_0,Z)}{N_0\Delta\Omega\Delta E}, \quad (2)$$

where $N(\theta,E,E_0,Z)$ is the number of electrons collected per unit time through an aperture subtending a solid angle $\Delta\Omega$ and in an energy interval ΔE. This measured ratio may be related to an idealized differential coefficient through the integral

$$G(\theta,E,E_0,Z)=\int_0^\infty \rho(\theta,E,\epsilon,Z)\phi(\epsilon,E_0)d\epsilon, \quad (3)$$

where

$$\rho(\theta,E,\epsilon,Z) = \frac{1}{\Delta\Omega\Delta E}\int_{E-\frac{1}{2}\Delta E}^{E+\frac{1}{2}\Delta E}\int_{\Delta\Omega}\oint\oint q(\mathbf{r})k[(\mathbf{p}-\mathbf{r}),\hat{a},E,\epsilon,Z] \times d^2r d^2p d\Omega dE. \quad (4)$$

Energy spectra of the retrofugal electrons are thus obtained by solving the integral Eq. (3) for ρ. Such energy spectra have been measured at incident energies E_0 from 1 to 10 MeV and for targets from $Z=6$ to 92. These results will be reported in a subsequent paper, but this paper will consider only the angular distribution and the total retrofugal-electron flux.

A coefficient describing the angular distribution is expressed ideally by

$$r(\theta,E_0,Z)=\int_0^\infty \rho(\theta,E,E_0,Z)dE, \quad (5)$$

whereas the actual measured quantity is

$$H(\theta,E_0,Z)=\int_{E_{\min}}^\infty G(\theta,E,E_0,Z)dE. \quad (6)$$

The difference between these is significant in two ways. First, the lower limit for the energy in Eq. (6) was established by the dimensions of the system and the earth's magnetic field which fixed $E_{\min}$ at about 800 eV. This low-energy cutoff is actually desirable since it discriminates against the secondary-emission electrons that leave the target surface in significant quantities but with energies below 50 eV. Negative bias voltages up to 300 V applied to the Faraday cup confirmed that no low-energy electrons were collected. Second, at the higher energies E_0, the measured coefficient G tends to be a little large compared with ρ because of the low-energy tail in the incident energy spectrum $\phi(\epsilon,E_0)$ as displayed in Fig. 4. Corrections for this have been evaluated and they run from approximately zero at 2 MeV for all targets to about 0.5% at 6 MeV and up to 1.2% for Be at 10 MeV which is the worst case. Consequently, the effect of the incident-electron energy spectrum has been reduced to an equivalent

monoenergy E_0 whose value is determined within $\pm 5\%$. Thus, after corrections, the values reported correspond closely to the coefficient $r(\theta,E_0,Z)$ as defined by Eq. (5). Evidently, $\rho(\theta,E,E_0,Z)$ is the value of $k[(\mathbf{p}-\mathbf{r}), \hat{a}, E, \epsilon, Z]$ averaged over the beam distribution illuminating the target area and over an interval of solid angle $\Delta\Omega$ centered about a direction $\hat{c}$ as well as over an energy interval ΔE centered about E.

An examination of the integral expressed in Eq. (4) reveals that the finite area irradiated by the incident beam tends to reduce the angular resolution of the measurement but introduces no other error provided the detector can receive retrofugal electrons from the entire region over which they issue from the target face. Since the solid angle is critical in these measurements it was determined very carefully. The solid angle subtended at the center of the target face by the detector aperture was $\Delta\Omega = 0.0096$ sr$\pm 1\%$. Any accidental misalignment would tend to reduce the effective solid angle and lead to measured results that are too low. The fact that one-half of the target face is closer and the other half farther from the detector aperture introduces an error that would cancel in first order for an incident beam uniformly filling the irradiated area. But since the incident beam actually had a cross-section diameter of about 2 mm and wandered over the permitted area whose diameter was 1 cm, an error of $\pm 5\%$ could be expected and is consistent with the variability in results actually observed. There is also a small systematic error introduced by choosing the geometrical $\Delta\Omega$ rather than an effective $\Delta\Omega$ determined from the integral of Eq. (4). This error is less than 1% and is variable, depending upon the position of the incident beam in the aperture. It would tend, also, to cause the final results to be too low. The angular positions θ were precisely determined by gauge stops within ± 10 min of arc, but because of the finite detector aperture the angular resolution was $\Delta\theta = \pm 3°$. Since the angular distributions are quite broad this resolution was entirely adequate.

EXPERIMENTAL RESULTS

Measurements of the retrofugal flux coefficient $r(\theta,E_0,Z)$ have been performed using targets of Be, C, Al, Cu, Sr, Mo, Ag, Ba, W, Pb, and U. The data cover an angular range from $\theta = 100°$ to 180° and an energy range from $E_0 \simeq 0.5$ to 10 MeV. These results are listed in Tables I through VIII and are displayed in Fig. 5 (a)–(g). The general consistency of the data and the progressive trends are evident. For Be, $r(\theta,E_0,4)$ drops rapidly with increasing energy; but as the target atomic number Z rises, the decrease in r with energy becomes less pronounced. Measurements at the angles $\theta = 100°$, 120°, 145°, and 155° were accomplished directly, but values indicated at $\theta = 180°$ could not be measured directly for obvious reasons. Instead, these were obtained through an experimental

TABLE I. Retrofugal electron flux coefficients $r(\theta,E_0,Z)$ for beryllium. Values are expressed in milliunits per steradian.

E_0 MeV	θ 180°	155°	145°	120°	100°
	±5%	±5%	±2%	±5%	±7%	±10%
0.68	5.52	4.70	4.14	2.48	0.73
0.90	5.06	4.51	4.45	2.14	0.72
1.18	4.71	3.84	3.91	1.99	0.55
1.50	4.10	3.44	3.18	1.69	0.38
1.98	3.40	2.88	2.58	1.35	0.19
3.20	2.48	2.12	1.87	1.18	0.16
3.92	2.23	1.81	1.66	1.08	0.08
4.31	2.14	1.62	1.51	1.02	0.03
4.95	1.69	1.55	1.38	0.88	0.02
5.67	1.67	1.38	1.17	0.78	0.05
6.48	1.38	1.26	1.17	0.76	0.05
7.42	1.41	1.18	1.09	0.81	0.08
8.35	1.26	1.19	1.07	0.83	0.06
9.28	1.28	1.12	1.03	0.73	0.06
9.76	1.19	1.13	0.99	0.73	0.04

TABLE II. Retrofugal electron flux coefficients $r(\theta,E_0,Z)$ for carbon. Values are expressed in milliunits per steradian.

E_0 MeV	θ 180°	155°	145°	120°	100°
	±5%	±5%	±5%	±5%	±7%	±10%
0.68	14.7	13.3	11.6	6.58	1.31
0.90	13.5	11.7	10.8	5.53	1.50
1.18	12.1	10.1	9.30	4.85	1.16
1.50	10.9	7.99	7.94	4.02	0.85
1.98	9.06	7.42	6.65	3.93	0.73
3.20	5.95	5.13	4.54	2.97	0.54
3.92	5.68	4.38	3.69	2.48	0.31
4.31	5.18	4.55	3.47	2.24	0.28
4.95	3.84	3.50	3.02	1.43	0.25
5.67	3.79	2.88	2.53	1.31	0.23
6.48	3.17	2.88	2.38	1.57	0.26
7.42	2.98	2.46	2.12	1.47	0.26
8.35	2.47	2.30	2.19	1.44	0.28
9.28	2.62	2.29	2.17	1.45	0.30
9.76	2.56	2.28	2.08	1.47	0.28

TABLE III. Retrofugal electron flux coefficients $r(\theta,E_0,Z)$ for aluminum. Values are expressed in milliunits per steradian.

E_0 MeV	θ 180°	155°	145°	120°	100°
	±5%	±5%	±5%	±5%	±7%	±10%
0.68	50.4	46.2	37.2	19.1	4.29
0.90	46.5	43.0	36.2	17.7	4.15
1.18	41.7	38.0	36.3	17.4	3.23
1.50	39.9	36.0	32.6	15.2	2.78
1.98	41.6	30.8	27.9	12.6	2.42
3.20	31.4	25.9	21.2	9.17	1.82
3.92	25.8	19.8	17.7	8.74	1.41
4.31	21.5	20.5	15.0	7.95	1.06
4.95	18.2	16.9	13.1	6.03	0.93
5.67	15.1	12.6	10.6	5.14	0.82
6.48	12.0	10.9	9.42	4.44	0.72
7.42	10.6	9.58	8.04	4.05	0.67
8.35	9.05	8.35	7.17	3.62	0.58
9.28	8.55	7.69	6.82	3.65	0.59
9.76	8.83	7.52	6.42	3.56	0.57

TABLE IV. Retrofugal electron flux coefficients $r(\theta,E_0,Z)$ for copper. Values are expressed in milliunits per steradian.

E_0 MeV	θ 180°	155°	145°	120°	100°
±5%	±5%	±2%	±5%	±5%	±10%
0.68		123	87.8	52.6	
0.90		114	90.5	48.8	
1.18	132	114	87.4	47.0	12.1
1.29	127		79.8		10.4
1.41	127	106	91.4		10.6
1.50	118	103	88.5	45.5	10.5
1.60	119	104	84.5		10.3
1.74	117	101	80.2		10.1
1.98	108	92.2	81.2	43.8	9.87
3.20	104	76.3	70.6	31.8	8.84
3.92	85.8	67.0	65.5	28.8	6.48
4.31	73.2	64.4	55.9	28.8	6.31
4.95	66.3	58.0	49.5	26.1	5.84
5.67	54.0	49.2	44.6	23.0	4.77
6.48	47.4	41.8	38.0	19.0	4.16
7.42	43.9	38.7	32.6	17.5	3.56
8.35	41.7	35.8	28.2	14.9	3.14
9.28	38.8	31.4	25.4	14.0	2.86
9.76	35.9	31.4	24.2	13.6	2.74

TABLE V. Retrofugal electron flux coefficients $r(\theta,E_0,Z)$ for silver. Values are expressed in milliunits per steradian.

E_0 MeV	θ 180°	155°	145°	120°	100°
±5%	±5%	±5%	±5%	±7%	±10%
0.68	199	168	146	65.8	17.3
0.90	199	174	141	63.0	15.4
1.18	190	155	156	68.8	14.0
1.50	184	155	142	67.8	14.6
1.98	178	169	130	72.7	13.2
3.20	161	124	116	65.2	11.5
3.92	136	100	105	59.2	10.4
4.31	127	124	95.0	47.8	9.22
4.95	108	90.3	84.8	35.1	8.13
5.67	97.0	76.1	75.6	30.3	7.43
6.48	86.0	79.9	67.4	34.0	6.62
7.42	80.7	69.3	57.2	31.0	6.10
8.35	74.3	65.2	57.3	27.6	5.85
9.28	71.7	60.4	52.2	25.3	5.52
9.76	69.0	62.1	51.5	24.0	5.20

TABLE VI. Retrofugal electron flux coefficients $r(\theta,E_0,Z)$ for lead. Values are expressed in milliunits per steradian.

E_0 MeV	θ 180°	155°	145°	120°	100°
±5%	±5%	±5%	±5%	±7%	±10%
0.68	258	228	201	106	24.9
0.90	263	232	210	103	22.0
1.18	254	220	214	115	21.4
1.50	244	222	198	101	20.1
1.98	247	200	198	104	18.9
3.20	228	188	165	92.3	17.2
3.92	208	174	158	79.8	15.1
4.31	195	170	143	73.5	14.5
4.95	170	152	133	63.5	13.5
5.67	158	132	121	58.7	12.6
6.48	147	128	117	58.5	11.4
7.42	137	119	107	50.6	10.9
8.35	126	113	101	52.4	10.0
9.28	120	106	94.6	53.0	9.98
9.76	117	98.6	90.9	49.1	9.84

TABLE VII. Retrofugal electron flux coefficients $r(\theta,E_0,Z)$ for uranium. Values are expressed in milliunits per steradian.

E_0 MeV	θ 180°	155°	145°	120°	100°
±5%	±3%	±2%	±3%	±5%	±10%
0.68	264	240	204	114	
0.90	276	241	214	116	
1.18	273	230	198	115	29.0
1.50	252	224	193	113	23.8
1.60			201	110	23.6
1.74			190	111	23.9
1.98	252	222	194	101	22.4
3.20	224	210	172	97.5	22.4
3.92	219	189	164	86.3	18.7
4.31	210	174	158	80.3	17.9
4.95	185	169	142	77.4	15.2
5.67	173	155	125	73.7	13.5
6.48	156	138	118	72.3	12.9
7.42	149	129	112	67.2	12.4
8.35	139	124	106	60.2	11.7
9.28	133	113	97.0	54.8	11.1
9.76	130	112	92.1	51.3	10.7

technique that avoids the problem of overlapping the incident beam. When a target is rotated so that the incident beam no longer strikes at normal incidence, the angular distribution profile of the retrofugal flux also shifts.[28] The maximum for this distribution moves in angle more rapidly than the angular displacement of the target and, in addition, increases in magnitude a few percent. The rate of angular shift and the rate of magnitude increase have been determined for each of the targets investigated. For example, with Be, the normal to the target must be set at 5° from the incident-beam axis in order to direct the maximum of the electron-flux distribution into the measurement port at 155°. At this angular offset, the maximum for the distribution is 8% greater than what it would have been at $\theta=180°$ with the primary beam at normal incidence. As Z for the target increases, the required

TABLE VIII. Retrofugal electron flux coefficients $r(\theta,E_0,Z)$ for strontium, molybdenum, barium, and tungsten. Values are expressed in milliunits per steradian. The incident beam is normal to the target, but the angle $\theta=155°$.

E_0 MeV	Target Sr	Mo	Ba	W
±5%	±5%	±5%	±5%	±5%
0.68	153	162	194	228
0.90	143	153	192	222
1.18	145	140	183	212
1.50	138	150	184	203
1.98	124	126	174	199
3.20	106	109	140	189
3.92	90.5	105	126	168
4.31	89.5	102	128	161
4.95	86.0	77.1	114	145
5.67	67.2	78.2	107	135
6.48	60.1	66.5	87.5	124
7.42	53.3	59.8	74.6	111
8.35	47.0	55.0	70.4	109
9.28	41.5	48.5	63.2	101
9.76	40.0	46.2	64.6	93.4

angular offset progressively increases while the magnitude correction becomes less. Accordingly, for a U target these values are 17.5° and 1.5%, respectively.

For a given target, the drop in $r(\theta,E_0,Z)$ with increasing incident electron energy E_0 can be understood in terms of the decline in the Coulomb scattering cross sections together with the relativistic tendency for all processes to go in the forward direction.[39] But as the target number Z increases, the decrease with energy becomes less pronounced. In addition, there is a qualitative change in the curve shape such that, in the vicinity of 3 MeV, an upward bow developes with increasing Z. These effects are consistent with increasing bremsstrahlung generation within a target and the attending increase in the energetic-secondary-electron component.

The development of $r(\theta,E_0,Z)$ as a function of target atomic number Z is most conveniently displayed at $\theta=180°$. These curves are shown in Fig. 6. The points indicated for each of the targets have been taken from the curves presented in Fig. 5 and from similar curves drawn from the data given in Table VIII. At small values of Z, $r(180°,E_0,Z)$ increases approximately with Z^2 in accord with the expected behavior of the scattering cross sections. For large Z, the curves tend to level off. This tendency also is expected since only a finite number of electrons will return from a finite number incident upon the target. Thus $r(180°,E_0,Z)$ would tend toward a finite limit even if the cross sections increased indefinitely with Z.

The general trend of $r(155°,E_0,Z)$ as a function of energy E_0 for the various targets Z is displayed in the family of curves given in Fig. 7. Here, the gradual development in the structure of the curves becomes evident and the progressive growth of an upward bow in the vicinity of 3 MeV is obvious. This detail again suggests the presence of secondary components that would tend to increase the basic retrofugal flux above that due to scattering alone.

Changes in the angular distributions of the retrofugal electrons from targets of low Z are indicated in Fig. 8. At low energies, the angular distributions tend toward cosine functions in agreement with the data of Kanter,[24] but they become sharper with increasing Z. Above 4 MeV, the angular distributions for these targets again become broader. Target materials having $Z>13$ are not included in Fig. 8, but they show angular distributions that are all approximately the same and effectively independent of energy. They are described by $\cos^{1.35}\theta$ and tend to follow the values expressed in Fig. 8 for Al at 8 MeV.

EVALUATION

A comparison of the results obtained from these measurements against those obtained by other investigators is important because of significant discrepancies that exist. In the present measurements the earth's magnetic field deflects the very low-energy electrons sufficiently to establish a low-energy cutoff at about 800 eV. This is consistent with the low-energy discrimination employed by others[22–33] although the present cutoff value is somewhat higher. It is possible to estimate the error introduced by such a low-energy cutoff from the energy spectra of the retrofugal electrons. These spectra have been measured for each of the targets and show behavior similar to that reported by Kulenkampff,[22,23] Kanter,[24] Sternglass,[40] and Frank.[28] The greatest error occurs for the highest incident energies and lowest Z because the resulting spectra have a relatively greater number of low-energy electrons. But even for a C target at $E_0=10$ MeV the error contributed by the cutoff at 800 eV much less than 0.1% and therefore completely negligible. A summary of results is presented in Fig. 9 where data and calculated values reported by previous investigators are superimposed upon curves derived from the present measurements. Much of the literature reports only the total retrofugal flux coefficient

$$R(E_0,Z)=\int_{2\pi} r(\theta,E_0,Z)d\Omega$$

obtained by integrating $r(\theta,E_0,Z)$ over the entire backward hemisphere. Therefore, the data in Fig. 9 are displayed in this form. The logarithmic energy scale is chosen partly for the convenience it affords in plotting the extended range in energy but also for emphasis at the low-energy values where most of the previous work has been done.

It is apparent immediately that nearly all of the results previously reported for energies above 30 keV lie below the present values although they exhibit the same general trend with energy. The present experimental values are listed in Tables IX and X and are represented by those portions of the continuous curves that fall above 0.5 MeV. These have been joined smoothly with the extensive data at lower energies obtained by Palluel[41] and by Sternglass.[40] Since no low-energy data for Pb and U are available, the pertinent curves have been extrapolated as indicated by the dotted lines. For energies above 10 MeV there is only a slow, steady decline as indicated by the measurements of Harder and Ferbert.[32] Thus, Fig. 9 displays the region in which $R(E_0,Z)$ has its most interesting development.

A Monte Carlo calculation of R by Green[19] shows excellent agreement with neighboring data. On the other hand, values calculated by Perkins[20] are about

[39] W. A. McKinley and H. Feshbach, Phys. Rev. **74**, 1759 (1948).

[40] E. Sternglass, Phys. Rev. **95**, 345 (1954).

[41] P. Palluel, Compt. Rend. **224**, 1492 (1947).

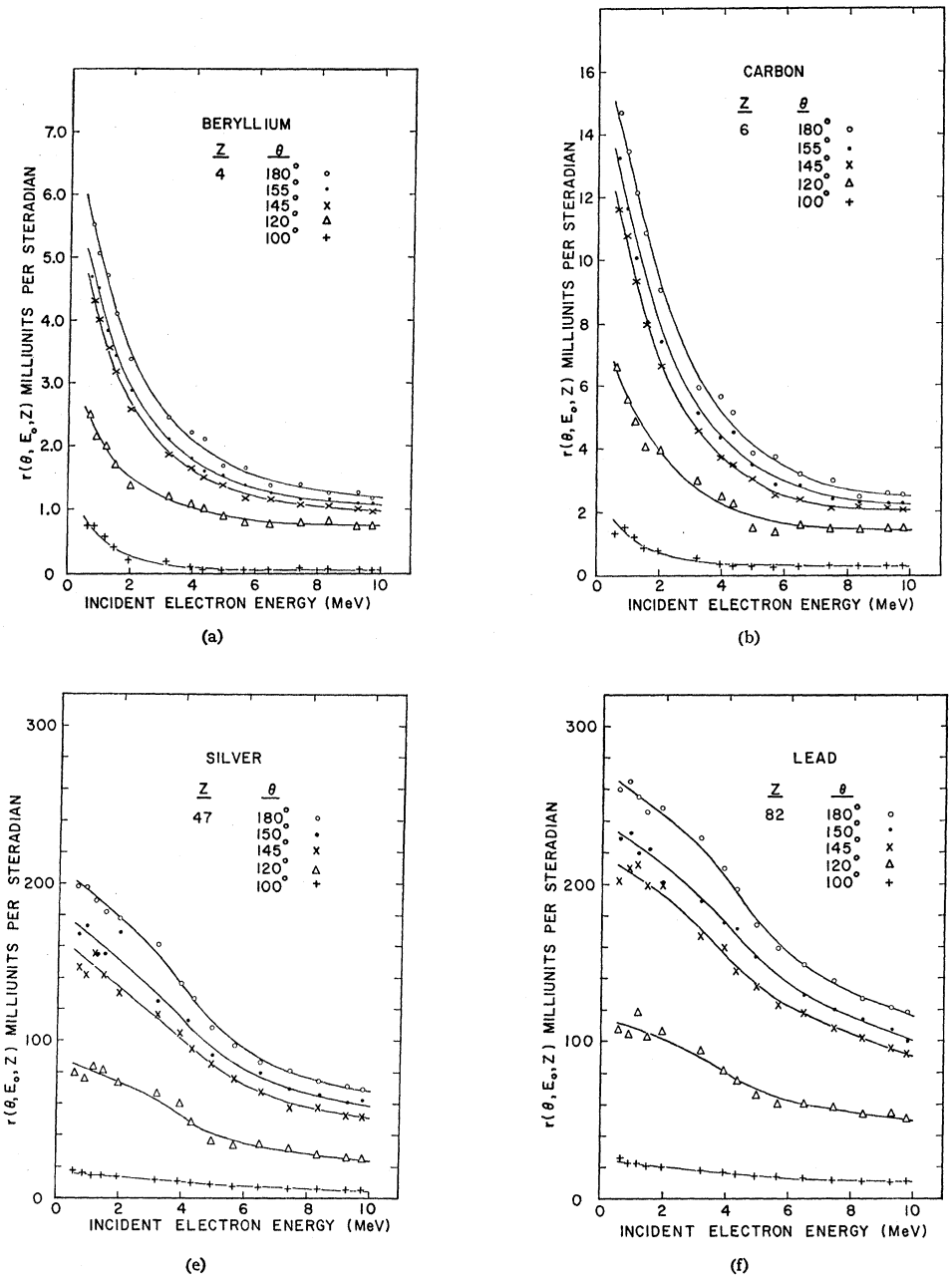

50% low compared with the present curves. These numbers contrast with the value obtained by Sidei, Higasimura, and Kinosita[17] for Al at 2.0 MeV which is about 40% higher than the present data. The calculations of Berger[21] for Al show the best agreement with the present measurements although they still fall about 20% below the indicated curves. All of the calculations performed to date have determined only the effects of scattering and energy loss but do not include the regeneration of energetic electrons due to secondary processes. Accordingly, the results would be expected to be low since energetic secondary electrons would add to the retrofugal flux. For the calculation performed by Green, however, contributions due to secondary effects are less important since the energy is very low. Hence the better agreement with the data is significant.

The possibility that the values reported by previous experimenters may be low is not surprising, for as Kulenkampff and Rüttiger[23] have pointed out, "Every operating influence serves to impose a reduction in the measured electron current." Recognizing this they confidently reported results which were larger than other values accepted at the time but which fit well into the

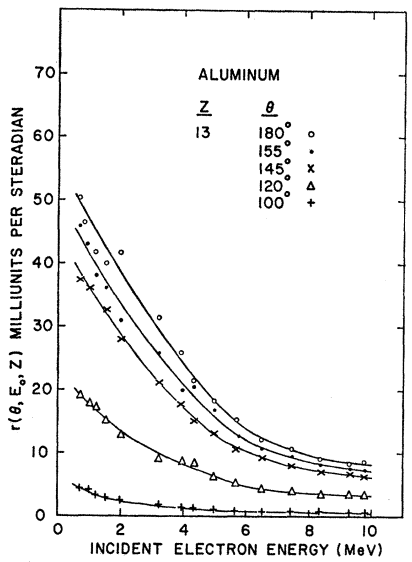

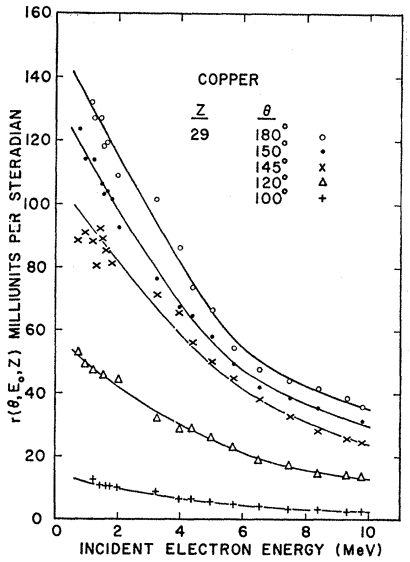

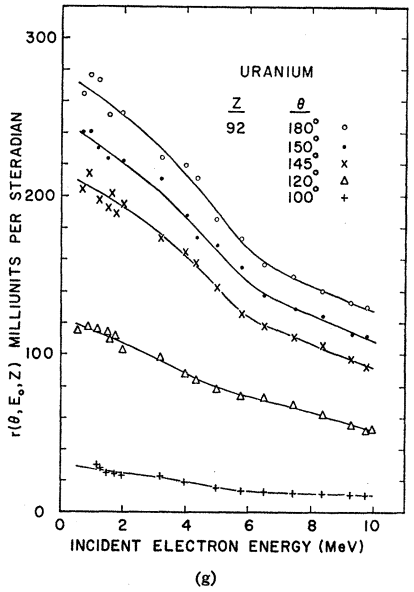

FIG. 5. Values of the retrofugal flux coefficient $r(\theta,E_0,Z)$ for various targets ranging from beryllium to uranium.

present scheme. Nevertheless, the consistent close agreement among the various independent investigators[28–33] regarding the magnitudes of the total coefficients for energies above 0.5 MeV is disturbing, especially when the discrepancy between their reported values and the present data is so large. Careful reexamination of every feature of the present measurement including the geometrical factors, instrument calibrations, and background levels has confirmed their magnitudes within the specified uncertainty limits. Moreover, the system has been completely disassembled and reassembled several times with entirely consistent results. Even the possibility that transient effects due to target charging during the short 0.03 nsec duration of the individual electron bunches delivered by the *S*-band Linac has been considered. But since, with the exception of carbon, the targets were all good conductors and since the average beam current per pulse was only about 15 mA, the target charging was negligible. Thus, there seems to be no identifiable source for a large error in the present measurements leading to a result that is too high.

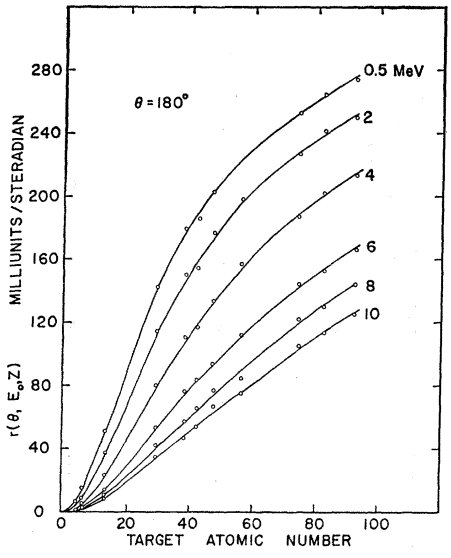

FIG. 6. Development of $r(\theta,E_0,Z)$ at $\theta=180°$ with increasing Z for various values of E.

On the other hand, it may be significant that most of the measurements by others were made with apparatus of nearly the same design and used similar materials in construction.[29–33] In each of these, the collector was an aluminum cup with a wide aperture facing the target. The incident electron beam was introduced through a small hole in the back of the collector. By this means, the total electron flux escaping from the target surface into the backward hemisphere was intercepted by the collector. However, this configuration places the collector directly in the strong scattered bremsstrahlung field issuing from the target.

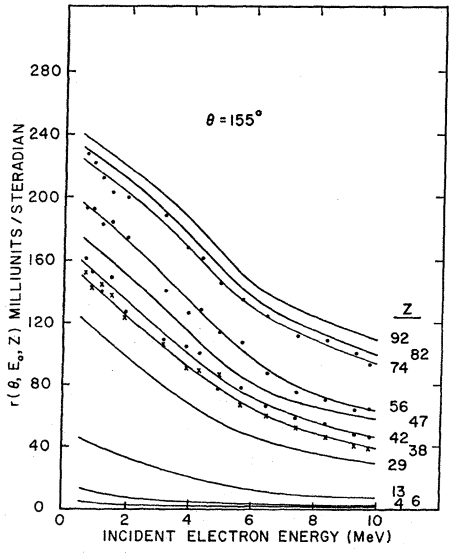

FIG. 7. Trend of $r(\theta,E_0,Z)$ at $\theta=155°$ with increasing values of Z. For clarity, experimental points have been suppressed except for the additional data on Sr, Mo, Ba, and W targets.

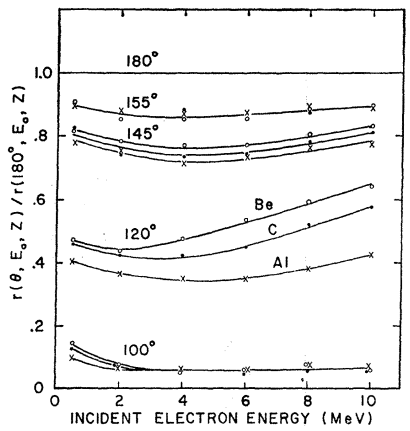

FIG. 8. Variation in the angular distribution of retrofugal flux from targets with low atomic number. Targets having atomic numbers $Z\geq29$ tend to have an angular distribution similar to that for Al at 8 MeV and are effectively independent of energy.

TABLE IX. Total retrofugal electron flux coefficients $R(E_0,Z)$. Values are expressed in milliunits.

E_0 MeV	Target Be	C	Al	Cu	Sr	Mo
±5%	±3%	±2%	±2%	±2%	±5%	±5%
0.68	16.1	43.8	133	348	468	495
0.90	15.5	39.2	125	334	437	468
1.18	13.7	33.7	115	334	443	428
1.50	11.5	28.3	107	313	422	458
1.98	9.50	27.8	98.5	286	379	385
3.20	7.27	17.1	75.2	248	324	324
3.92	6.55	15.0	61.7	216	276	321
4.31	6.06	14.5	55.7	195	273	312
4.95	5.09	11.0	46.6	176	262	236
5.67	5.03	9.81	38.2	150	205	238
6.48	4.68	9.62	32.2	128	187	203
7.42	4.81	8.85	28.6	116	163	183
8.35	4.75	8.57	25.2	106	143	168
9.28	4.78	9.00	23.9	96.0	130	148
9.76	4.68	9.00	23.8	92.0	122	141

TABLE X. Total retrofugal electron flux coefficients $R(E_0,Z)$. Values are expressed in milliunits.

E_0 MeV	Target Ag	Ba	W	Pb	U
±5%	±2%	±5%	±5%	±2%	±2%
0.68	511	593	697	700	724
0.90	506	586	679	709	745
1.18	500	560	648	704	721
1.50	482	562	621	672	689
1.98	482	532	608	658	673
3.20	409	428	578	589	620
3.92	350	385	514	543	577
4.31	345	391	492	512	545
4.95	278	348	444	458	503
5.67	244	327	413	412	462
6.48	234	267	379	394	425
7.42	208	228	339	364	401
8.35	196	215	333	342	376
9.28	184	193	308	329	350
9.76	180	197	285	313	336

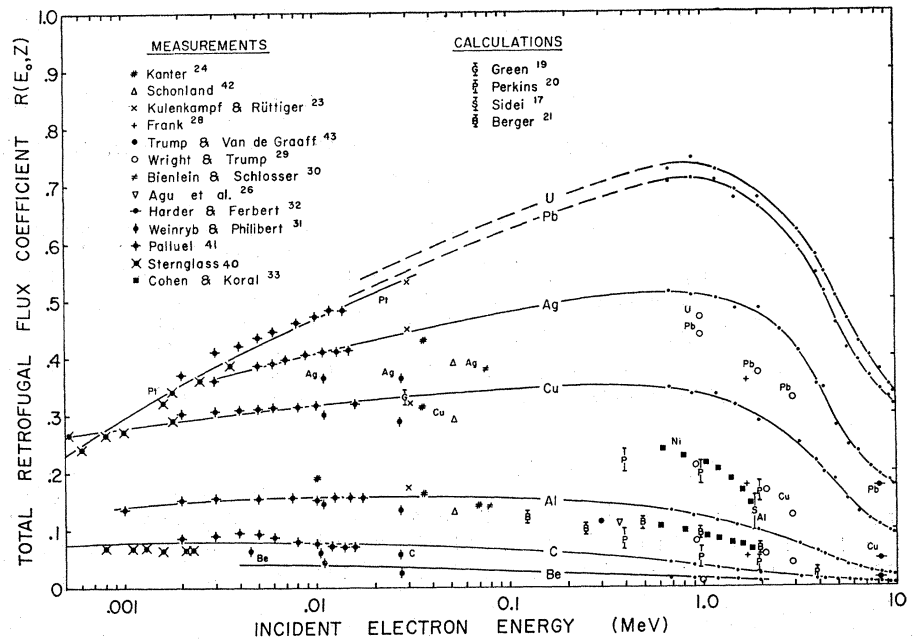

FIG. 9. Summary of results obtained by various investigators for the total retrofugal flux coefficient $R(E_0,Z)$. The latter portions of the continuous curves are derived from the present data while the points are labeled according to the authors reporting them. Smooth connections have been made with the low-energy data except for Pb and U for which no low-energy data exist. In these cases dashed curves have been drawn.

In view of the positive charge that accumulated on the Faraday cup when irradiated broadside with bremsstrahlung, as described earlier, it is quite likely that significant charge losses occurred from the outer walls of these collectors. The Faraday cup used for the present measurements was designed to minimize such losses. It had a carbon liner about 3 cm thick and this was encased within a similar thickness of lead as shown in Fig. 1. When an electron beam enters this cup from the front in the normal manner the subsequent charge loss from the outer walls for energies less than 10 MeV is smaller than 0.2%. But when, for a test, the cup was deliberately irradiated broadside with target bremsstrahlung it then acquired a positive charge of magnitude comparable to the negative charge normally collected from the retrofugal electrons. For this reason, the cup was set far back from the target and carefully shielded from broadside irradiation by stray bremsstrahlung from the Linac. The error from this cause was thereby reduced to the small magnitude previously quoted. However, the collectors employed by the other investigators were not shielded from the target bremsstrahlung and except for the apparatus of Harder and Ferbert[32] the wall thicknesses employed were not sufficient to attenuate the bremsstrahlung very much. Under these conditions the charge losses could lead to errors as large as 20 to 30% which is enough to account for the observed discrepancy. Moreover, since the charge losses would increase with the target atomic number Z, the fractional error would roughly be constant. This seems to be consistent with the observed relationship to the present data.

In the measurements reported by Frank,[28] a pair of Geiger tubes operated in coincidence as a directional detector were used. Although the data were taken at deliberately low counting rates and corrections for counting losses were applied, there is still a possibility that additional counting losses occurred. Frank used a betatron operating at 500 Hz and having an electron pulse duration of about 10 μsec. Because of the Geiger-tube dead time, there could be no more than 1 count per pulse. Therefore, if one or the other of the Geiger tube pair were triggered by secondary electrons ejected from the surrounding detector shield it would not register a count but nevertheless would block the detector system during the remainder of that pulse. These secondary electrons again would be associated with the scattered target bremsstrahlung. It seems plausible that these spurious events were numerous, otherwise there would be no need for the directional advantage of a coincidence counter pair. Accordingly, Frank's results also would be expected to be low.

Data reported recently by Koral and Cohen[33] show that targets thicker than one-half the electron range approximate an infinite thickness very well. The targets chosen for the present measurements all were thicker than the full electron range at 10 MeV, which was the highest energy employed. Therefore, for all of the incident-electron energies used, the targets effectively were infinitely thick.

ACKNOWLEDGMENTS

Appreciation is expressed for the assistance of Antonio Grijalva for keeping the Linac in excellent condition and to Albert Saxman who participated in collecting some of the data.

[42] B. F. J. Schonland, Proc. Roy. Soc. (London) **108**, 187 (1924).
[43] J. Trump and R. Van de Graaff, Phys. Rev. **75**, 44 (1949).